BioEnergy Research (2021) 14:322–332
https://doi.org/10.1007/s12155-020-10155-2

Fundamental Insights into Walnut Shell Bio-Oil Electrochemical Conversion: Reaction Mechanism and Product Properties

Xinhua Yuan[1] · Xiefei Zhu[1] · Liqiang Zhang[1] · Zejun Luo[1] · Xifeng Zhu[1]

Received: 19 March 2020 / Accepted: 14 June 2020 / Published online: 9 July 2020

Abstract

The potential for electrochemical conversion of bio-oil was overlooked for a long period due to the poor electrical conductivity and unclear reaction mechanism. This study aimed to provide an insight into bio-oil of electrochemical conversion mechanism and product distribution. In this study, using walnut shell bio-oil with enhanced electrical conductivity by ammonium carbonate as raw material, electrolysis experiments were carried out using different electrolysis times by constant current method (20 mA) in H-type electrolytic cell at a stable temperature (0 °C). The results showed that phenols, aldehydes, and lignin were copolymerized; meanwhile, unsaturated fatty acids such as oleic acid underwent decarbonylation and decarboxylation. The hydrogen-releasing electrode reaction also occurred at the cathode during the conversion process. Besides, the properties of products were characterized by elemental analysis, GC-TCD/FID, GC/MS, ^{1}H NMR, FTIR, and TG-FTIR. Solid products were of possibility for application in new materials owing to containing copolymers with lignin structure, and gas products could be utilized as gas fuels with the combustible gas (H_2, CO, CH_4, and olefins) content as 79.24%.

Keywords Electrochemical conversion · Copolymerization · Decarbonylation · Decarboxylation · Electrode reaction · Hydrogen

Introduction

Considering the risk of fossil fuel depletion and pollution to the environment, bio-oil, a pyrolysis product from sustainable biomass sources with zero net CO_2 emission and better transport property, becomes a promising option and attracts more and more interest. It can be applied in combustion or chemical processing because it is a mixture of hundreds of organic compounds containing important chemical raw materials and high value-added chemical components including acids, ketones, aldehydes, phenols, ethers, esters, sugars, and furans [1–4]. However, such complexity in components, high water content, high viscosity, strong corrosivity, and poor thermal stability, have brought various technical difficulties in its applications [5]. Consequently, many methods have been developed by researchers for bio-oil upgrading, such as supercritical fluids, esterification, catalytic cracking, hydrogenation, molecular distillation, hydrodeoxygenation, emulsification, and catalytic pyrolysis [6–11]. These methods have alleviated some practical application problems like high viscosity and hard to combustion. Nevertheless, many other problems are still waiting to be resolved, such as harsh application conditions, difficulty in control, high equipment cost, and low conversion rates. Therefore, it is necessary and meaningful to explore more potential upgrading methods.

Compared with the above upgrading methods, electrochemical conversion, which plays a pivotal role in the production of some organic products and metals such as adiponitrile, phthalate, Al, Na, K, and Li, might have been overlooked in bio-oil upgrading [12, 13]. As a mature industrial method, electrochemical conversion has many obvious advantages [14]. For instance, it requires no extreme conditions or special heating and pressure equipment; its reaction speed even species can be changed effectively and continuously by controlling the electrode potential; its product is easy to separate and has high purity, causing low environmental pollution. As early as 1983, Bargon et al. [15] studied the polymerization of aromatic compounds through electrochemical synthesis. Bernardo et al. [16] believed that biomass could be the material for electrochemical synthesis because of the abundant aromatic polymer lignin, one of the most effective and renewable sources of aromatic compounds. This shows the potential of electrochemical conversion in the application of bio-oil.

✉ Xifeng Zhu
xfzhu@ustc.edu.cn

[1] Department of Thermal Science and Energy Engineering, University of Science and Technology of China, 96 Jinzhai Road, Hefei 230026, Anhui, People's Republic of China

Furthermore, hydrogen, a clean and highlighted energy, can also be produced in the electrochemical conversion processes of bio-oil. Presently, hydrogen production can be achieved by hydrocarbon reforming, hydrocarbon pyrolysis, biomass process, and water splitting [17, 18]. Among these methods, water splitting seems to be a feasible way to produce large quantities of hydrogen stably and efficiently because of the easy access and pollution-free to raw materials. Therefore, the high water content in bio-oil provided an available source for hydrogen production through electrocatalysis [19, 20]. Thus, even the high water content and the complex aromatic compounds in bio-oil, which have been so far always a hindrance to the application of bio-oil, may turn out to be the merits of bio-oil in electrochemical synthesis and preparation of hydrogen. Hence, this method is expected to greatly facilitate the application of bio-oil.

However, the electrochemical conversion demands an in-depth understanding of the reaction mechanism. Unfortunately, despite this encouraging potential, the reaction mechanism was unclear due to the poor electrical conductivity and complex components. This leaves bio-oil electrochemical synthesis groundless and obstructs the further application of bio-oil. Therefore, this study aims to provide a basic understanding of the bio-oil electrochemical conversion mechanism based on product properties and reaction processes.

In this study, the electrical conductivity of walnut shell bio-oil was enhanced by ammonium carbonate, avoided the appearance of ion metals in bio-oil. The electrolysis device was designed based on H-type electrolytic cell to electrolyze the processed bio-oil by constant current method (20 mA) at a stable temperature (0 °C). The products were collected according to different electrolysis time, consisting of residual bio-oil, gas products, and solid products. The residual bio-oil was analyzed by ^{1}H NMR, GC/MS, and elemental analyzer to study the change of functional groups and compounds in the process. Additionally, to study the chemical compositions and product properties, gas products were determined by GC-TCD/FID and solid products were detected by FTIR and TG-FTIR. The reaction mechanism was deduced by studying the change of functional groups and components of products.

Materials and Methods

Materials

Bio-oil was prepared by pyrolysis of the walnut shell at 500 °C in a fluidized bed, with the condensing temperature at 40–50 °C. Walnut shell is produced in Ningguo, Anhui Province, and content of cellulose, hemicellulose, and lignin was 22.06 wt%, 19.90 wt%, and 53.81 wt% respectively. The pyrolysis details were reported in our previous study [21]. The elemental analysis and determination of water content were preformed to bio-oil. The analysis was conducted with an Elementar Vario EL-III analyzer. Besides, the content of O was calculated by the difference. The water content was determined by the Karl–Fischer titration. The titration solvent was a mixture of chloroform and methanol at the mass ratio of 1:3, and the accuracy of the results was checked by water addition. Besides, in this study, the high heating value (HHV) was calculated from the elemental compositions (Eq. 1) [22]. The result was showed in Table 1.

$$\mathrm{HHV(MJ/kg)} = 1.87\left(\mathrm{C}^2\right) - 144(\mathrm{C}) - 2802(\mathrm{H}) + 63.8(\mathrm{CH}) + 129(\mathrm{N}) + 20147 \quad (1)$$

The compounds in bio-oil were mainly weak electrolytes and non-electrolytes, which resulted in the poor conductivity of bio-oil [23]. The conductivity would have a great influence on the effect of electrolysis. However, the metal ion in most salts would go against the process of application bio-oil. Therefore, a small amount of ammonium carbonate (0.48 g/100 ml) was added to the bio-oil to enhance the electrical conductivity (ammonium carbonate (AR) is produced by Sinopharm Chemical Reagent limited corporation).

Electrolysis Device and Experiment

Figure 1 shows the schematic diagram of the experimental device for electrolysis. According to the previous literature, a two-electrode system with a divided H-type electrolytic cell was designed [24, 25]. The power supply was adjustable (100 V/1 A dc), and the size of the electrode was 10 × 10 × 0.1 mm. After adding ammonium carbonate and stirring for 24 h, it is filtered several times to remove impurities and precipitates from the bio-oil. Before the experiment, the prepared bio-oil (94.15 g/100 mL) was put into the electrolytic cell, which had been immersed in an ice-water mixture to maintain a constant temperature. N_2 (concentration, 99.999%) was used as the carrier gas, and the gas flow was 20 mL/min, swept out for 30 min. The electrolysis time was set to 6, 12, 18, and 24 h at 20 mA (the current was limited by equipment) respectively, to study the effect of different electrolysis time.

After electrolysis, a thick black gel appeared at the bottom of the electrolytic cell and gas products were also generated, collected by the gas collector. However, because there were few gas products with short electrolysis time, the gas products for 24 h were collected and analyzed, named GP. Classified according to different electrolysis time, the bio-oils were named RB-0, RB-6, RB-12, RB-18, and RB-24 (collectively called RB). Correspondingly, the thick black gels, dried in the oven at 50 °C for 24 h, were named SP-6, SP-12, SP-18, and SP-24 (collectively called SP).

Table 1 Characterization of walnut shell bio-oil

Name (wt%)	N	C	H	O[a]	Water content	HHV (MJ/kg)
Bio-oil	2.02±0.09	23.88±0.34	6.83±0.12	67.27±0.21	30.93±0.24	9.32

[a] Calculated by the difference

Analytical Methods

^{1}H NMR Analysis

^{1}H NMR analysis was implemented on RB. The nuclear magnetic resonance (NMR) spectroscopy was operated at room temperature on a Bruker 400 MHz liquid nuclear magnetic resonance apparatus. For ^{1}H NMR, about 20 mg of the sample was dissolved in 0.5 mL of deuterated dimethyl sulfoxide (DMSO-d6), and tetramethylsilane (TMS) was used as the internal standard. Experimental parameters were listed: 30° pulse angle, 1-s relaxation delay, and 300 K test temperature [26].

GC/MS Analysis

RB was analyzed by GC/MS (Trace DSQII, Thermo Scientific, USA), coupled with the TG-5 MS chromatographic column. The split ratio was 40:1, and the carrier gas was helium (concentration, 99.999%). The inlet temperature, ion source, and transmission line temperature were set to 280 °C. The heating procedure of the furnace box was to hold for 2 min at 40 °C, then rose to 180 °C at the rate of 3 °C/min and held for 2 min, and finally rose to 280 °C at 10 °C/min and held for 3 min [27].

The electron ionization (EI) voltage and the scanning range of the mass spectrometry were set to 70 eV and 45–650 amu (atomic mass unit) respectively. To ensure the repeatability of the experiment, each test was repeated three times, and the results were analyzed with the average value of the experiment.

Elemental and Bio-Chemical Analysis

RB was analyzed for their elemental compositions, and the analysis of elemental and bio-chemical compositions was conducted to SP. The element detection procedure was the same as the bio-oil. After treatment with neutral detergent [28], the two-stage acid hydrolysis (2 mol/L HCl and 75 wt% H_2SO_4) was performed on the sample. The lignocellulosic contents were determined by using gravimetric methods [29, 30].

GC-TCD/FID Analysis

The gas chromatograph (GC1690) equipped with TCD (thermal conductivity detector) and FID (hydrogen flame ion detector) was used for the detection and analysis of GP. The equilibrium gas of the standard mixture was nitrogen, and the other main effective components were CO_2, H_2, CH_4, C_2H_4, C_2H_6, C_3H_6, C_4H_8, and C_4H_{10}, respectively.

FTIR Analysis

The functional groups of SP were detected by FTIR through pelleting the sample with KBr powder. The Nicolet 8700 Fourier transform infrared spectrometer was used for infrared spectroscopy, with a resolution of 4 cm^{-1}, 32 scanning times, and a wavenumber of 4000–400 cm^{-1} [31].

TG-FTIR Analysis

TG-FTIR was performed on SP by a thermogravimetric analyzer (TGA, Q500, TA Instruments, USA) with N_2 as the carrier gas and a flow rate of 100 mL/min. The speed of equilibrium gas flow was 20 mL/min, and the temperature increased from 30 to 800 °C at the rate of 20 °C/min.

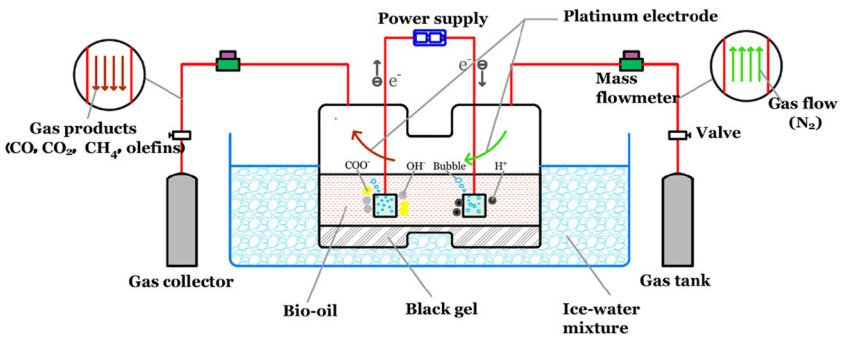

Fig. 1 Schematic diagram of the electrolysis device

Results and Discussion

Yield Analysis

The yields of RB, GP, and SP with different electrolysis time were shown in Fig. 2, and the yield of GP was calculated by the difference. The presence of GP revealed that hydrogen might be released in the electrolysis process, which was the common product in electrochemical reactions. As we saw, the yields of GP reached 15.53% with 24 h electrolysis time, and the increase was 3.70%, 4.98%, 3.78%, and 3.07% in each stage. It indicated that the growth rate of GP increased in the first 12 h, and then decrease. It could be speculated that there might be multiple gas release reactions, some of which occurred mainly in the first 12 h. Another interesting product was SP, which might be the product of polymerization of compounds in bio-oil, such as phenols, aldehydes, lignin, and furans. It had a marked decrease in the growth of SP, which was reduced from 0.72 to 0.05% in the process. It demonstrated that the rate of reactions to produce SP was decreased, which might be attributed to the reduction of reactants. When the reactants ran out, the growth rate of SP had a rapid decrease, which resulted in the inconspicuous differences in the yield of 18 h and 24 h. Therefore, by comparing the yield and growth rates of GP and SP, it could be obtained that the gas releasing reactions taken place at all times, and the growth rate peaked at 12 h in the process of electrolysis, while the rate of the reactions that produced solids decreased with the extension of time.

Residual Bio-Oil Analysis

GC/MS Analysis of Residual Bio-Oil

RB was analyzed by GC/MS, and the compounds with relative concentrations higher than 0.5% were screened out in Table 2. It showed that the compounds in bio-oil produced by walnut shells contained acids, furans, phenols, and aldehydes. It could be found that the content of phenols was relatively high in bio-oil. This might originate from the raw material, walnut shell, which has lower cellulose and hemicellulose content and much higher lignin [32]. It could be found there was a remarkable change in the content of acids, furans, and phenols after electrolysis. A rapid decrease in the content of furfural, trans-m-propylene guaiacol, and phenol in RB-6 appeared, compared with RB-0. According to the result of yield analysis, the yield of SP had a rapid increase at first 6 h. Both Long et.al [33] and Wu et.al [34] found that there could be a polymerization between phenols and furfural to produced aerogels in acidic conditions. It indicated that the reactions between furfural and phenols might be the source of SP, and the gels collected from the bottom of the electrolytic cell might contain the product of copolymerization in SP. Additionally, the content of some phenols kept decreasing in 6 to 18 h, such as 4-ethyl-2-methylphenol and 4-allyl-2-methoxyphenol, which might due to the copolymerization of phenols, aldehydes, and lignin [35–38]. The adequate lignin in walnut shell provides sufficient raw materials for the copolymerization reaction. In the meantime, a gradual increase

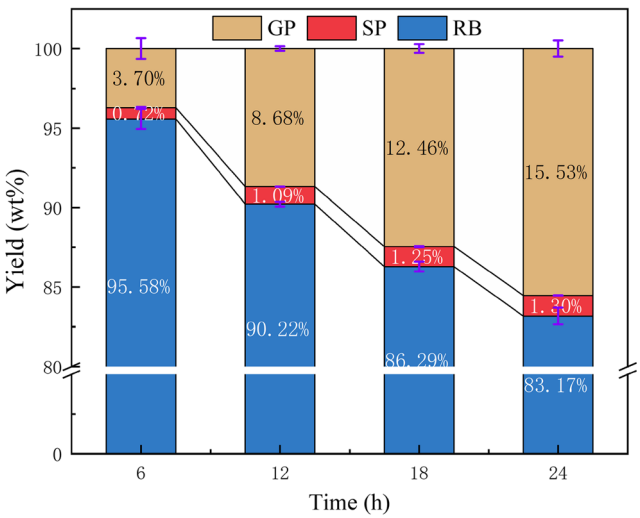

Fig. 2 Yields with different electrolysis time

Table 2 The compounds in RB

Compounds	Peak area/%				
	RB-0	RB-6	RB-12	RB-18	RB-24
Acetic acid	7.24	10.58	12.18	9.66	15.82
Glycol aldehyde diethyl acetal	3.67	3.08	3.50	2.74	4.66
Furfural	2.12	0.33	0.34	0.39	0.55
2,5-Dimethoxytetrahydrofuran	3.04	3.86	3.95	4.00	3.86
Trimethoxybutane	0.70	0.97	1.10	1.10	1.33
Phenol	2.79	1.76	2.08	1.97	2.01
O-cresol	1.89	1.65	1.62	1.68	1.59
Guaiacol	6.58	6.65	7.05	6.88	7.11
Hexanal dimethyl acetal	1.40	1.73	1.63	1.57	1.34
3,4-Dimethylphenol	2.01	1.61	1.55	1.45	1.48
Naphthalene	0.55	0.55	0.42	0.54	0.24
P-hydroxyphenyl ethanol	1.59	0.55	1.43	0.61	0.53
2-Methoxy-4-methylphenol	3.92	4.97	5.15	4.72	4.65
4-Ethyl-2-methylphenol	1.50	1.54	1.03	0.78	0.99
4-Ethyl-2-methoxyphenol	3.17	4.05	4.19	3.96	3.70
2,6-Dimethoxyphenol	2.03	2.17	2.19	2.02	1.95
4-Allyl-2-methoxyphenol	2.21	2.63	2.52	2.39	2.29
Phenol, 2-methoxy-4-propyl-	1.20	1.37	1.23	1.13	0.87
Trans-m-propylene guaiacol	3.16	1.44	1.45	1.77	1.38
Isoeugenol	6.28	7.03	6.94	7.11	5.81
5-Tert-butyl pyrogallol	1.41	2.30	2.53	1.76	3.24
4-Allyl-2,6-dimethoxyphenol	1.19	3.22	3.09	3.25	2.68
Oleic acid	2.50	2.25	1.08	1.21	0.27

appeared in the relative content of many substances, such as trimethoxybutane, guaiacol, and 5-tert-butyl pyrogallol. It was due to the amount of bio-oil decreased as the electrolytic reaction progressed; therefore, the content of those substances that did not participate in the reaction increased. Consequently, it can be inferred that two factors were affecting the content of phenols. One was the decrease because of the copolymerization; the other was the relative increase due to the decrease of bio-oil.

Another noteworthy finding was that, with longer electrolysis time, the oleic acid concentration declined. It demonstrated that decomposition might happen to oleic acid in the electrolysis process. It was found that the deoxygenation of the carboxyl group in oleic acid could be achieved by releasing CO, CO_2, and H_2O via decarbonylation, decarboxylation, and dehydration mechanisms, which will also produce light olefins [39]. In the process, the carboxyl group transformed into the hydrocarbon and formic acid via deoxygenation, and formic acid decomposition can occur via two parallel pathways, namely, dehydration to CO and H_2O and dehydrogenation to CO_2 and H_2 [40]. Therefore, according to this hypothesis, GP might contain CO, CO_2, and some olefins.

^{1}H NMR Analysis of Residual Bio-Oil

The proton NMR spectra and the integral values of selected regions of the spectra on a percentage basis of RB were shown in Fig. 3, and the integral values of different regions could represent the proton number of different functional groups. The organic functional groups according to the chemical shift range were presented in Table 3. From the spectra, it could be found that the functional groups of samples were similar, including extended alkyl chains, carbonyl group, aromatic group, and aldehyde group. However, some interesting changes took place in the integral values of different regions. As we saw, an opposite trend could be found out in both regions of 4.4–3.3 ppm and 3.3–2.3 ppm, which were the two regions with the highest integral value. The region of 4.4–3.3 ppm (~ 50% of all protons) could represent protons on carbon atoms next to the aliphatic alcohol or methylene group that joins two aromatic rings, which would exist in lignin structures [4, 26]. In the first 6 h, the decrease of the proton number and the methoxy group in RB was due to the copolymerization reaction of phenols. In the meantime, with the copolymerization and dehydration reaction going on, the water content would keep increasing, and the result had a good match with it [36, 40].

About the region of 3.3–2.3 ppm (~ 35% of all protons), it could represent aliphatic protons attached to carbon atoms adjacent to a carbonyl or aromatic group. A slight increase in the integral value was due to the decrease of bio-oil in the first 6 h. However, when the oleic acid content reduced, as seen in the 6–24 h, the decrease of the integral value of this region was because of the decarbonylation reaction of the

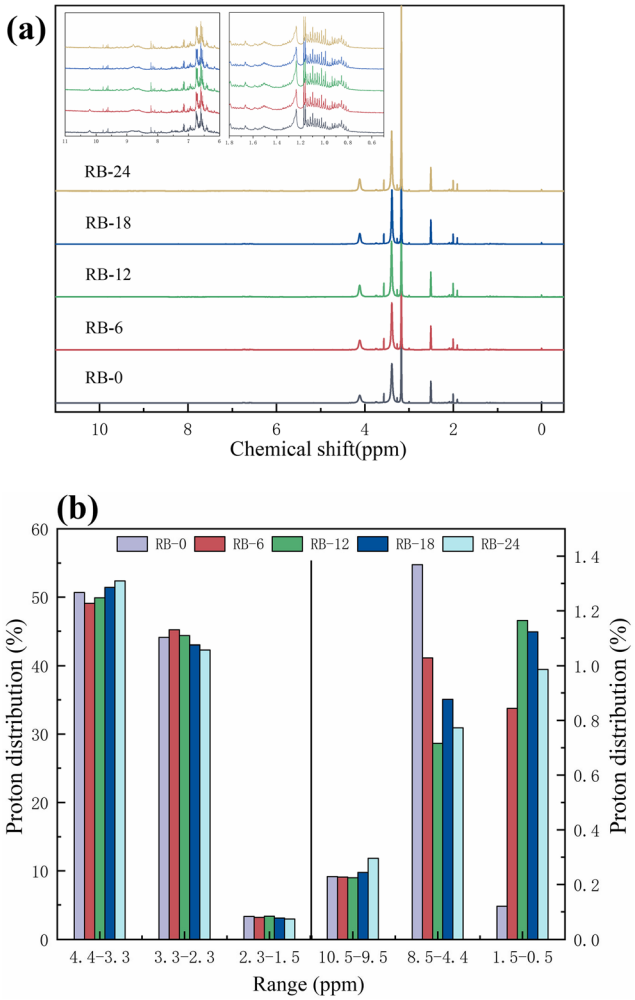

Fig. 3 ^{1}H NMR spectra of RB and integral values of selected regions: **a** ^{1}H NMR spectra of RB; **b** integral values of selected regions of the spectra of RB

methoxy group. Similarly, the change of the region (1.5–0.5 ppm) represented extended alkyl chains and was attributed to the decomposition of unsaturated fatty acids like oleic acid. The integral value of region (2.3–1.5 ppm) was stable, which indicated that the protons attached to carbon atoms adjacent to a carbon–carbon double bond or a carbonyl and aromatic group might not participate in the electrochemical conversion.

Elemental Composition and Water Content Analysis of Residual Bio-Oil

The data of RB elemental composition and water content were collected, and the results were presented in Table 4. It could be found that the content of O was relatively high because of the existence of water and acid, over 60%, which led to the relatively low HHV of RB [41]. In the first 12 h, the HHV of RB was sharply decreasing. It was due to the large release of combustible gas, such as H_2, CO, and CH_4. Furthermore, a gradual drop appeared in the number of C. It was due to the

Table 3 Proton assignment according to chemical shift range

Chemical shifts (ppm)	Proton assignment
0.5–1.5	Aliphatic protons in extended alkyl chains
1.5–2.3	Protons attached to carbon atoms adjacent to a carbon–carbon double bond or a carbonyl and aromatic group
2.3–3.3	Aliphatic protons attached to carbon atoms adjacent to a carbonyl or aromatic group
3.3–4.4	Protons attached to carbon atoms singly bonded to oxygen, and protons in water
4.4–8.5	Aromatic protons, carbon–carbon double bond
9.5–10.5	Protons in aldehyde group and carboxyl of acids

generation of solid products and gas products such as aerogels, CO, and CO_2, via the copolymerization and the deoxygenation of the carboxyl group. In the meantime, the increase in water content was also owing to these reactions. Another noticing thing was that the marked change in the content of H. In the first 6 h, the mass formation of the SP led to a rapid decline in the content of C and O, resulting in a rise in the content of H. However, in 6 h to 24 h, the steady fall in the content of H might be due to the release of H_2 and olefins [39].

Gas Products Analysis

It was essential to analyze the composition of GP whether to determine the type of reaction or the mechanism of the reaction. The components of GP were determined by GC-TCD/FID. The results showed that there were CO, CO_2, H_2, CH_4, and olefins in GP, and the contents reached 38.66%, 20.76%, 35.51%, 0.72%, and 4.35% respectively. It could be obtained that CO, CO_2, and H_2 were the main gas products, and the combustible gas (H_2, CO, CH_4, and olefins) content in GP reached 79.24%. It also showed the great potential of GP in gaseous fuel. In terms of the reaction mechanism, one of the main reactions of the gas releasing was the reduction of hydrogen ions at the cathode to hydrogen [42]. Hussain et al. [43] also found that hydrogen evolution was more likely to occur on platinum electrodes during electrolysis. Meanwhile, hydrogen can also be released by dehydration of formic acid [40]. Besides, the generation of CO_2 could be divided into two parts. For one thing, some CO_2 was released by the reaction of carbonate and free hydrogen ions that were produced by the anodic reaction [44]; for another, the deoxygenation of the carboxyl group could also produce CO_2 [45]. The deoxygenation reaction in bio-oil was also the major source of CO and olefins [39]. As for the CH_4, it was believed, under the catalysis of platinum, CO_2 could be reduced to CO_2^-, which could react with hydronium to produce CH_4 [46]. In the meantime, CH_4 could also be generated by demethylation [47].

Solid Products Analysis

Elemental Compositions and Bio-Chemical Analysis of Solid Products

The elemental compositions, HHV and O/C ratios of SP were presented in Table 5. The results showed the C content of all the samples was stable and relatively high, over 70%. It might be due to the abundant aromatic ring structures in the copolymerization products, which contained adequate carbon [48]. It could be found out that there were mainly lignin oligomers in SP, and the content of cellulose and hemicellulose was relatively low. It was because most cellulose and hemicellulose in biomass are broken down, and lignin is converted to phenols and lignin oligomers in the pyrolysis process of biomass [4]. The O/C ratio can depict a characteristic trend for aromaticity measurements because it traces closely the median of all aromatic measurements and thereby shows a typical pattern for aromaticity [49]. The O/C ratio was increased with the

Table 4 Elemental composition and water content of RB

Name (wt%)	N	C	H	O[a]	Water content	HHV (MJ/kg)
RB-0	4.18 ± 0.18	27.45 ± 0.16	7.25 ± 0.05	61.12 ± 0.37	31.72 ± 0.16	10.52
RB-6	4.06 ± 0.12	27.18 ± 0.22	8.25 ± 0.07	60.51 ± 0.33	31.94 ± 0.19	9.33
RB-12	1.76 ± 0.09	25.98 ± 0.03	7.68 ± 0.08	64.58 ± 0.14	32.78 ± 0.03	9.11
RB-18	1.97 ± 0.02	25.12 ± 0.05	7.34 ± 0.06	65.57 ± 0.08	32.74 ± 0.06	9.16
RB-24	2.25 ± 0.06	23.46 ± 0.07	6.64 ± 0.06	67.65 ± 0.07	34.09 ± 0.08	9.42

[a] Calculated by the difference

Table 5 Elemental compositions and bio-chemical analysis of SP

	SP-6	SP-12	SP-18	SP-24
N (wt%)	3.24 ± 0.08	3.01 ± 0.28	2.07 ± 0.22	2.13 ± 0.02
C (wt%)	70.79 ± 0.38	70.63 ± 0.72	71.33 ± 0.78	70.27 ± 0.26
H (wt%)	6.13 ± 0.39	6.22 ± 0.11	6.17 ± 0.02	6.25 ± 0.19
O[a] (wt%)	19.84 ± 0.07	20.14 ± 0.77	20.43 ± 0.87	21.35 ± 0.16
Cellulose (wt%)	2.29 ± 0.12	2.42 ± 0.15	2.12 ± 0.09	2.15 ± 0.04
Hemicellulose (wt%)	3.01 ± 0.15	3.25 ± 0.05	3.10 ± 0.25	3.05 ± 0.08
Lignin (wt%)	85.58 ± 0.17	85.43 ± 0.22	86.02 ± 0.38	86.07 ± 0.36
HHV (MJ/kg)	30.25	30.29	30.45	30.04
O/C[b]	0.280	0.285	0.286	0.304

[a] Calculated by the difference

[b] Atomic ratio

extension of electrolysis time, indicating the increase of aromaticity in SP. It was worth noting that a slight increase appeared in HHV of SP before 18 h; however, it turned to a drop at 24 h. It demonstrated that if high HHV was required in SP, unquestionable, 18 h was an appropriate electrolytic time.

FTIR Analysis of Solid Products

The functional groups of SP were analyzed by FTIR, and the IR spectra of SP were shown in Fig. 4. No significant difference between these infrared curves was found. It indicated there was no marked change in the category of the major functional groups in SP during the electrochemical conversion processes. Furthermore, it could be seen that the significant characteristic band of 3440–3200 cm^{-1} was attributed to the stretching vibration of –OH [29]. The increasing peak intensity indicated the increase of the carboxyl group in SP. The absorption peak at 3000–2820 cm^{-1} related to the stretching vibration of $–CH_2$ and $–CH_3$, demonstrating the existence of hydrocarbon compounds, which might be the product of the decomposition of oleic acid. What's more, the absorption peaks at 1612, 1514, and 1368 cm^{-1} were attributed to the stretching vibration of C=C, C–C, and C–H, respectively, originating from the skeleton of the aromatic ring [31]. The absorption peak at 1375 cm^{-1} and 1250 cm^{-1} represented the symmetrical variable angles of C–H and the stretching of C–O respectively, indicating that SP contained R-OH structure. The gradual rise was found in the intensity as a consequence of copolymerization, which also proved from the side that SP contained phenols copolymerization products. This also corresponded to the gradual increase of aromaticity in SP in elemental analysis. Another absorption peak was found at 885–820 cm^{-1}, representing the lateral curvature of the carbonate. The carbonate might be derived from the addition of ammonium carbonate. The decline of the peak intensity was due to the reaction of carbonate and free hydrogen ions.

TG-FTIR Analysis of Final Solid Product

SP-24, as the final solid product, was selected to analyze the pyrolysis properties. Both TG (in wt%) and DTG (in wt%/min) curves were shown in Fig. 5. It could be observed that a significant weight loss peaks, in which SP loss 60% mass, appeared in DTG curve of SP-24 between 50 and 600 °C, which reached the maximum mass loss rate (0.89 wt%/°C) at 170 °C and maintained until 350 °C. Generally, the weight loss process could be divided into three stages [50]. The first stage was between 30 and 200 °C, due to the evaporation of moisture and small molecules. The second stage was between temperatures of approximately 200 °C and 600 °C, owing to the cracking of the polymer backbones and the thermal degradation of the components with lignin structures. The third stage was at 660 °C, attributed to the dissociation of diaryl ethers at higher temperatures and secondary pyrolysis of volatiles [51]. Additionally, there was still a 40% solid residue left at 800 °C after pyrolysis. In the previous study, the lignin

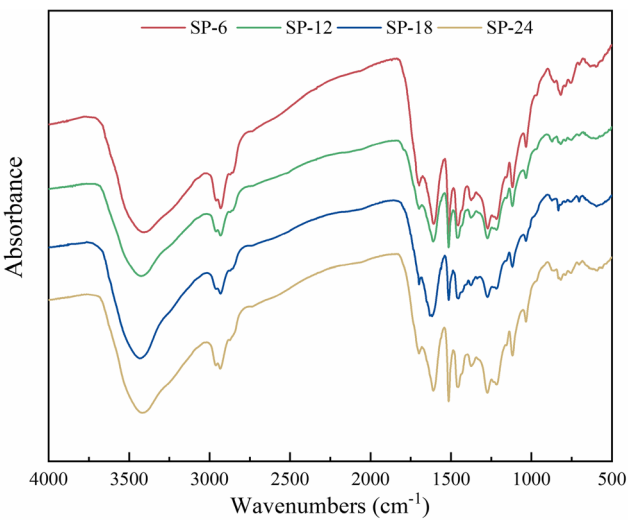

Fig. 4 FTIR spectra of SP

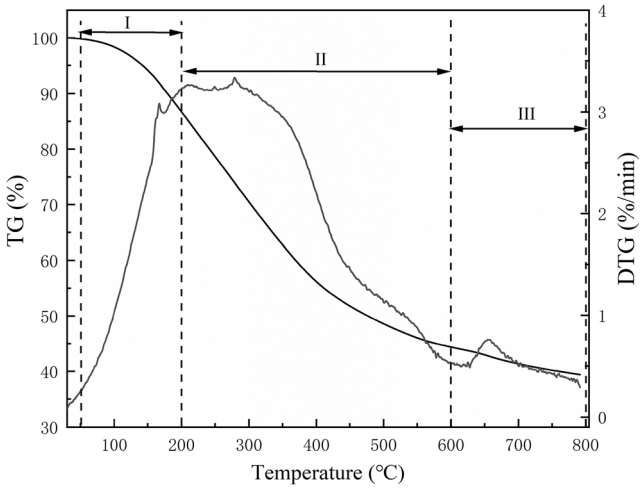

Fig. 5 TG-DTG curves of SP-24

structure has the characteristics of slow decomposition at high temperatures [26, 52]. Hence, the residues might be the carbon and incomplete pyrolytic copolymer with lignin structures.

Figure 6 shows the IR absorption spectra of the gases produced by SP-24 at several representative temperatures in the pyrolysis process. Two hundred, 300, and 650 °C were the temperatures at different stages of pyrolysis, and 400 °C was the point with the fastest decreases in the weight loss rate. It could be found that the main gas products were H_2O (3965–3500 cm^{-1}), CH_4 (3100–2780 cm^{-1}), CO_2 (2360–2310 cm^{-1}), CO (2180–2110 cm^{-1}), and methanol (1085–970 cm^{-1}), according to the relationship between wavenumbers and products [51]. Among them, CH_4 could be the product of the release of the weak key methoxyl and methylene CH_2 fracture. The cleavage of carbonxyl and carboxyl groups was the source of CO_2, and CO could originate from the dissociation of diaryl ether and the secondary pyrolysis of volatiles at high

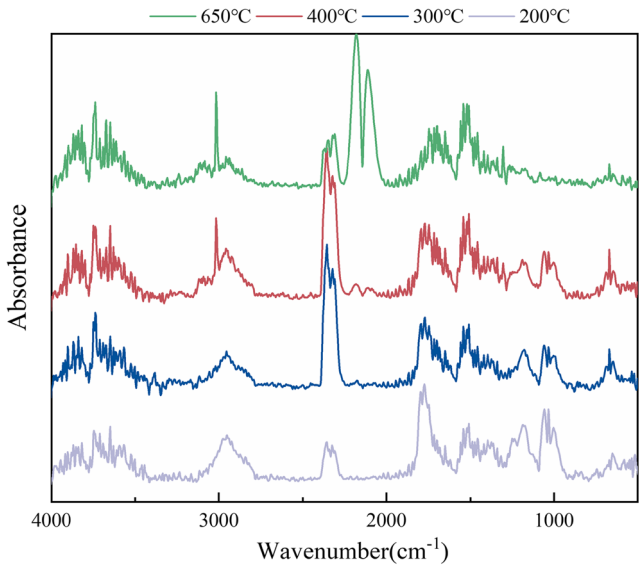

Fig. 6 The infrared spectra of the gas products produced from SP-24 at different temperatures

temperature. Generally, the methoxyl substituents in the lignin structures might be the source of methanol [53]. Based on Lambert–Beer law, absorbance has a linear relationship with gas concentration at a specific wavenumber [54]. Therefore, the change of absorbance in the whole process related to the changing trend of gas product yield. The absorption peaks at 1880–1640 cm^{-1} and 1300–1100 cm^{-1} were related to the absorption of C=O bond and R–OH respectively. With higher temperatures, a significant decrease appeared in both of them, which was due to the reduction in the number of carboxyl groups and phenols. On the contrary, the absorption band at 1605–1370 cm^{-1}, which represented the C=C bond attributed to the aromatic component, was increased with higher temperatures. It was owing to the increase in the degree of aromatization. Below 400 °C, the absorption peaks represented CO at 2180–2110 cm^{-1} did not appear, and a marked increase could be found in the intensity of this absorption peaks at 650 °C. It was owing to a large amount of energy requirement in dissociation of diaryl ether and the secondary pyrolysis of volatiles.

A Proposed Reaction Mechanism for Bio-Oil Electrochemical Conversion

To understand the electrochemical conversion process of the bio-oil more clearly, basing on the above discussions, the main reactions involved during the electrolysis of the bio-oil are summarized in Fig. 7. In the process of electrolysis, the copolymerization of phenols, aldehydes, and lignin, the decarbonylation and decarboxylation of unsaturated fatty acids and the splitting of water occurred in the bio-oil. The solid products were generated by the copolymerization; however, with the increase of reaction time, the growth rate was decreased because of the exhaustion of reactants. Therefore, the copolymerization mainly occurred at 0–12 h. The gas products consist of CO, CO_2, H_2, CH_4, and olefins. Among that, CO, CO_2, and olefins were mainly from the decarbonylation and decarboxylation of unsaturated fatty acids. Furthermore, the reaction of carbonate and free hydrogen ions could also produce CO_2. And H_2 and CH_4 were produced by the reduction at the cathode.

Conclusion

In the process of bio-oil electrochemical conversion, three kinds of products were collected: residual bio-oil, gas products, and copolymerized solids. The results showed that there were several major reactions during electrolysis: the copolymerization between phenols, furfural, and lignin, the decarbonylation and the decarboxylation of unsaturated fatty acids like oleic acid, and reduction of hydrogen ions at the cathode. Among them, the decarbonylation and the decarboxylation of unsaturated fatty acids and the reduction of

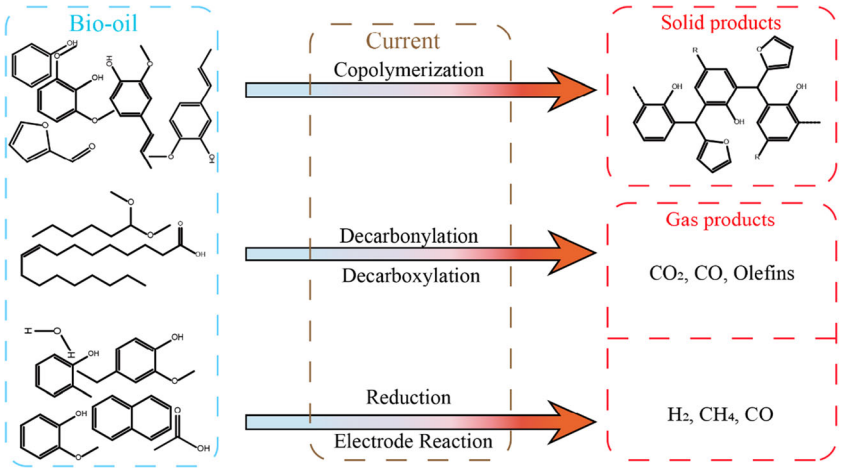

Fig. 7 A proposed reaction mechanism for bio-oil electrochemical conversion

hydrogen ions were the major sources of gas products. The gas releasing reactions took place at all times, and the growth rate peaked at 12 h due to the decarbonylation and decarboxylation reaction. Due to the depletion of reactants such as furfural and phenols, copolymerized solids yields increased first and then reached an upper limit at 18 h. Additionally, both solid and gas products exhibited promising properties. Copolymerized solids with lignin structure and gas products containing 79.24% combustible gas content could be possible to apply to new materials and gas fuels respectively.

This present work displayed the basic understanding of bio-oil electrochemical conversion mechanism and the promising product properties. It showed the great potential in the electrochemical conversion of bio-oil, providing the foundation for the further bio-oil application.

Funding Information This work was funded by the National Natural Science Foundation of China (No. 51676179).

References

1. Wang C, Luo Z, Diao R, Zhu X (2019) Study on the effect of condensing temperature of walnut shells pyrolysis vapors on the composition and properties of bio-oil. Bioresour Technol 285: 121370. https://doi.org/10.1016/j.biortech.2019.121370
2. Hayerly MR, Okoren KV, Brown RC (2016) Thermal stability of fractionated bio-oil from fast pyrolysis. Energy Fuel 30(11):9419–9426. https://doi.org/10.1021/acs.energyfuels.6b01606
3. Hu X, Gholizadeh M (2019) Biomass pyrolysis: a review of the process development and challenges from initial researches up to the commercialisation stage. J Energ Chem 39:109–143. https://doi.org/10.1016/j.jechem.2019.01.024
4. Saikia P, Gupta UN, Barman RS, Kataki R, Chutia RS, Baruah BP (2015) Production and characterization of bio-oil produced from *Ipomoea carnea* bio-weed. Bioenerg Res 8(3):1212–1223. https://doi.org/10.1007/s12155-014-9561-2
5. Kim JS (2015) Production, separation and applications of phenolic-rich bio-oil - a review. Bioresour Technol 178:90–98. https://doi.org/10.1016/j.biortech.2014.08.121
6. Yang W, Li X, Zhang D, Feng L (2017) Catalytic upgrading of bio-oil in hydrothermal liquefaction of algae major model components over liquid acids. Energy Convers Manag 154:336–343. https://doi.org/10.1016/j.enconman.2017.11.018
7. Agarwal A, Park S-J, Park J-H (2019) Upgrading of kraft lignin-derived bio-oil over hierarchical and nonhierarchical Ni and/or Zn/HZSM5 catalysts. Ind Eng Chem Res 58(51):22791–22803. https://doi.org/10.1021/acs.iecr.9b05348
8. Zhou M, Zeng Z, Zhu H, Xiao G, Xiao R (2014) Aqueous-phase catalytic hydrogenation of furfural to cyclopentanol over Cu-Mg-Al hydrotalcites derived catalysts: model reaction for upgrading of bio-oil. J Energ Chem 23(1):91–96. https://doi.org/10.1016/s2095-4956(14)60109-1
9. Xie H, Yu Q, Yao X, Duan W, Zuo Z, Qin Q (2015) Hydrogen production via steam reforming of bio-oil model compounds over supported nickel catalysts. J Energy Chem 24(3):299–308. https://doi.org/10.1016/s2095-4956(15)60315-1
10. Saber M, Nakhshiniev B, Yoshikawa K (2016) A review of production and upgrading of algal bio-oil. Renew Sust Energ Rev 58: 918–930. https://doi.org/10.1016/j.rser.2015.12.342
11. Cheng S, Wei L, Julson J, Rabnawaz M (2017) Upgrading pyrolysis bio-oil through hydrodeoxygenation (HDO) using non-sulfided Fe-Co/SiO2 catalyst. Energy Convers Manag 150:331–342. https://doi.org/10.1016/j.enconman.2017.08.024
12. Pletcher D, Walsh FC (2012) Industrial electrochemistry. Springer Science & Business Media, Berlin
13. Newman J, Thomas-Alyea KE (2012) Electrochemical systems. John Wiley & Sons, Hoboken
14. Brett C (2004) Fundamentals of electrochemistry. In: Arnau Vives A (ed) Piezoelectric transducers and applications. Springer, Berlin Heidelberg, pp 185–194. https://doi.org/10.1007/978-3-662-05361-4_11
15. Bargon J, Mohmand S, Waltman RJ (1983) Electrochemical synthesis of electrically conducting polymers from aromatic-compounds. IBM J Res Dev 27(4):330–341. https://doi.org/10.1147/rd.274.0330
16. Frontana-Uribe BA, Little RD, Ibanez JG, Palma A, Vasquez-Medrano R (2010) Organic electrosynthesis: a promising green methodology in organic chemistry. Green Chem 12(12):2099–2119. https://doi.org/10.1039/c0gc00382d
17. Nikolaidis P, Poullikkas A (2017) A comparative overview of hydrogen production processes. Renew Sust Energ Rev 67:597–611. https://doi.org/10.1016/j.rser.2016.09.044
18. Chun YN, Song HW, Kim SC, Lim MS (2008) Hydrogen-rich gas production from biogas reforming using plasmatron. Energy Fuel 22(1):123–127. https://doi.org/10.1021/ef700302z
19. Fei H, Dong J, Arellano-Jimenez MJ, Ye G, Dong Kim N, Samuel EL, Peng Z, Zhu Z, Qin F, Bao J, Yacaman MJ, Ajayan PM, Chen D, Tour JM (2015) Atomic cobalt on nitrogen-doped graphene for

hydrogen generation. Nat Commun 6:8668. https://doi.org/10.1038/ncomms9668
20. Nguyen T, Abdin Z, Holm T, Mérida W (2019) Grid-connected hydrogen production via large-scale water electrolysis. Energy Convers Manag 200:112108. https://doi.org/10.1016/j.enconman.2019.112108
21. Wang C, Ding H, Zhang Y, Zhu X (2020) Analysis of property variation and stability on the aging of bio-oil from fractional condensation. Renew Energy 148:720–728. https://doi.org/10.1016/j.renene.2019.10.159
22. Dhyani V, Bhaskar T (2018) A comprehensive review on the pyrolysis of lignocellulosic biomass. Renew Energy 129:695–716. https://doi.org/10.1016/j.renene.2017.04.035
23. Arnold S, Rodriguez-Uribe A, Misra M, Mohanty AK (2018) Slow pyrolysis of bio-oil and studies on chemical and physical properties of the resulting new bio-carbon. J Clean Prod 172:2748–2758. https://doi.org/10.1016/j.jclepro.2017.11.137
24. Marshall RJ, Walsh FC (1985) A review of some recent electrolytic cell designs. Surf Technol 24(1):45–77. https://doi.org/10.1016/0376-4583(85)90015-9
25. Zhu H, Wang L, Chen Y, Li G, Li H, Tang Y, Wan P (2014) Electrochemical depolymerization of lignin into renewable aromatic compounds in a non-diaphragm electrolytic cell. RSC Adv 4(56):29917–29924. https://doi.org/10.1039/c4ra03793f
26. Zhu WZ, Theliander H (2015) Precipitation of lignin from softwood black liquor: an investigation of the equilibrium and molecular properties of lignin. BioResources 10(1):1696–1714
27. Zhang L, Li S, Ding H, Zhu X (2019) Two-step pyrolysis of corncob for value-added chemicals and high-quality bio-oil: effects of alkali and alkaline earth metals. Waste Manag 87:709–718. https://doi.org/10.1016/j.wasman.2019.03.002
28. Vansoest PJ, Wine RH (1967) Use of detergents in analysis of fibrous feeds .4. determination of plant call-wall constituents. J Assoc Off Anal Chem 50(1):50-&
29. Abnisa F, Arami-Niya A, Daud WMAW, Sahu JN (2013) Characterization of bio-oil and bio-char from pyrolysis of palm oil wastes. Bioenerg Res 6(2):830–840. https://doi.org/10.1007/s12155-013-9313-8
30. Sluiter JB, Ruiz RO, Scarlata CJ, Sluiter AD, Templeton DW (2010) Compositional analysis of lignocellulosic feedstocks. 1. Review and description of methods. J Agric Food Chem 58(16):9043–9053. https://doi.org/10.1021/jf1008023
31. Zhu X, Luo Z, Diao R, Zhu X (2019) Combining torrefaction pretreatment and co-pyrolysis to upgrade biochar derived from bio-oil distillation residue and walnut shell. Energy Convers Manag 199:111970. https://doi.org/10.1016/j.enconman.2019.111970
32. Yaman E, Yargic AS, Ozbay N, Uzun BB, Kalogiannis KG, Stefanidis SD, Pachatouridou EP, Iliopoulou EF, Lappas AA (2018) Catalytic upgrading of pyrolysis vapours: effect of catalyst support and metal type on phenolic content of bio-oil. J Clean Prod 185:52–61. https://doi.org/10.1016/j.jclepro.2018.03.033
33. Long DH, Zhang J, Yang JH, Hu ZJ, Li TQ, Cheng G, Zhang R, Ling LC (2008) Preparation and microstructure control of carbon aerogels produced using m-cresol mediated sol-gel polymerization of phenol and furfural. New Carbon Mater 23(2):165–170. https://doi.org/10.1016/S1872-5805(08)60020-7
34. Wu D, Fu R (2006) Synthesis of organic and carbon aerogels from phenol–furfural by two-step polymerization. Microporous Mesoporous Mater 96(1–3):115–120. https://doi.org/10.1016/j.micromeso.2006.06.022
35. Zhang W, Ma Y, Wang C, Li S, Zhang M, Chu F (2013) Preparation and properties of lignin-phenol-formaldehyde resins based on different biorefinery residues of agricultural biomass. Ind Crop Prod 43:326–333. https://doi.org/10.1016/j.indcrop.2012.07.037
36. Blinkovsky AM, Dordick JS (1993) Peroxidase-catalyzed synthesis of lignin phenol copolymers. J Polym Sci A Polym Chem 31(7):1839–1846. https://doi.org/10.1002/pola.1993.080310722
37. Popp JL, Kirk TK, Dordick JS (1991) Incorporation of para-cresol into lignins via peroxidase-catalyzed copolymerization in nonaqueous media. Enzym Microb Technol 13(12):964–968. https://doi.org/10.1016/0141-0229(91)90118-t
38. Vazquez G, Gonzalez J, Freire S, Antorrena G (1997) Effect of chemical modification of lignin on the gluebond performance of lignin-phenolic resins. Bioresour Technol 60(3):191–198. https://doi.org/10.1016/s0960-8524(97)00030-8
39. Li FW, Ding SL, Li L, Gao C, Zhong Z, Wang SX, Li ZX (2016) Catalytic pyrolysis of model compounds and waste cooking oil for production of light olefins over La/ZSM-5 catalysts. 2016 International Conference on New Energy and Future Energy System (Nefes 2016) 40. Unsp 012072https://doi.org/10.1088/1755-1315/40/1/012072
40. Santillan-Jimenez E, Crocker M (2012) Catalytic deoxygenation of fatty acids and their derivatives to hydrocarbon fuels via decarboxylation/decarbonylation. J Chem Technol Biotechnol 87(8):1041–1050. https://doi.org/10.1002/jctb.3775
41. Thangalazhy-Gopakumar S, Adhikari S, Ravindran H, Gupta RB, Fasina O, Tu M, Fernando SD (2010) Physiochemical properties of bio-oil produced at various temperatures from pine wood using an auger reactor. Bioresour Technol 101(21):8389–8395. https://doi.org/10.1016/j.biortech.2010.05.040
42. Kundu A, Sahu JN, Redzwan G, Hashim MA (2013) An overview of cathode material and catalysts suitable for generating hydrogen in microbial electrolysis cell. Int J Hydrog Energy 38(4):1745–1757. https://doi.org/10.1016/j.ijhydene.2012.11.031
43. Hussain J, Jonsson H, Skulason E (2016) Faraday efficiency and mechanism of electrochemical surface reactions: CO2 reduction and H2 formation on Pt(111). Faraday Discuss 195:619–636. https://doi.org/10.1039/c6fd00114a
44. Zeng K, Zhang D (2010) Recent progress in alkaline water electrolysis for hydrogen production and applications. Prog Energy Combust Sci 36(3):307–326. https://doi.org/10.1016/j.pecs.2009.11.002
45. Ahmadi M, Macias EE, Jasinski JB, Ratnasamy P, Carreon MA (2014) Decarboxylation and further transformation of oleic acid over bifunctional, Pt/SAPO-11 catalyst and Pt/chloride Al2O3 catalysts. J Mol Catal A: Chem 386:14–19. https://doi.org/10.1016/j.molcata.2014.02.004
46. Tahir M, Amin NS (2015) Indium-doped TiO_2 nanoparticles for photocatalytic CO_2 reduction with H_2O vapors to CH_4. Appl Catal B-Environ 162:98–109. https://doi.org/10.1016/j.apcatb.2014.06.037
47. Joffres B, Nguyen MT, Laurenti D, Lorentz C, Souchon V, Charon N, Daudin A, Qignard A, Geantet C (2016) Lignin hydroconversion on MoS2-based supported catalyst: comprehensive analysis of products and reaction scheme. Appl Catal B-Environ 184:153–162. https://doi.org/10.1016/j.apcatb.2015.11.005
48. Hsiue GH, Shiao SJ, Wei HF, Kuo WJ, Sha YA (2001) Novel phosphorus-containing dicyclopentadiene-modified phenolic resins for flame-retardancy applications. J Appl Polym Sci 79(2):342–349. https://doi.org/10.1002/1097-4628(20010110)79:2<342::Aid-app180>3.3.Co;2-#
49. Wiedemeier DB, Abiven S, Hockaday WC, Keiluweit M, Kleber M, Masiello CA, McBeath AV, Nico PS, Pyle LA, Schneider MPW, Smernik RJ, Wiesenberg GLB, Schmidt MWI (2015) Aromaticity and degree of aromatic condensation of char. Org Geochem 78:135–143. https://doi.org/10.1016/j.orggeochem.2014.10.002

50. Long T, Li M, Chen YX, Zhu XF (2014) Study on evaporation characteristics of bio-oil and its compound models. BioResources 9(3):4242–4252
51. Zhu XF, Zhang YM, Ding HZ, Huang LR, Zhu XF (2018) Comprehensive study on pyrolysis and co-pyrolysis of walnut shell and bio-oil distillation residue. Energy Convers Manag 168:178–187. https://doi.org/10.1016/j.enconman.2018.05.012
52. Yang HP, Yan R, Chen HP, Lee DH, Zheng CG (2007) Characteristics of hemicellulose, cellulose and lignin pyrolysis. Fuel 86(12–13):1781–1788. https://doi.org/10.1016/j.fuel.2006.12.013
53. Liu Q, Wang S, Zheng Y, Luo Z, Cen K (2008) Mechanism study of wood lignin pyrolysis by using TG-FTIR analysis. J Anal Appl Pyrolysis 82(1):170–177. https://doi.org/10.1016/j.jaap.2008.03.007
54. Zhao LC, Guo MH, Li XD, Huang YP, Wu SH, Sun JJ (2017) Molar range detection based on sideband differential absorption spectroscopy with a concentrated reference. Anal Chem 89(24):13429–13433. https://doi.org/10.1021/acs.analchem.7b03722